

## Prediction of silicon-based room temperature quantum spin Hall insulator via orbital mixing

This content has been downloaded from IOPscience. Please scroll down to see the full text.

2016 EPL 113 67003

(<http://iopscience.iop.org/0295-5075/113/6/67003>)

View [the table of contents for this issue](#), or go to the [journal homepage](#) for more

Download details:

IP Address: 159.226.35.16

This content was downloaded on 15/04/2016 at 01:38

Please note that [terms and conditions apply](#).

# Prediction of silicon-based room temperature quantum spin Hall insulator via orbital mixing

HUIXIA FU<sup>1</sup>, JUN REN<sup>2,3</sup>, LAN CHEN<sup>1</sup>, CHEN SI<sup>2</sup>, JINGLAN QIU<sup>1</sup>, WENBIN LI<sup>1</sup>, JIN ZHANG<sup>1</sup>, JIATAO SUN<sup>1</sup>, HUI LI<sup>1</sup>, KEHUI WU<sup>1,3</sup>, WENHUI DUAN<sup>2,3</sup> and SHENG MENG<sup>1,3(a)</sup>

<sup>1</sup> *Beijing National Lab for Condensed Matter Physics & Institute of Physics, Chinese Academy of Sciences Beijing 100190, China*

<sup>2</sup> *Department of Physics, Tsinghua University - Beijing 100084, China*

<sup>3</sup> *Collaborative Innovation Center of Quantum Matter - Beijing 100190, China*

received 3 November 2015; accepted in final form 29 March 2016

published online 13 April 2016

PACS 73.22.-f – Electronic structure of nanoscale materials and related systems

PACS 71.70.Ej – Spin-orbit coupling, Zeeman and Stark splitting, Jahn-Teller effect

**Abstract** – The search for realistic materials capable of supporting the room temperature quantum spin Hall (QSH) effect remains a challenge, especially when compatibility with the current electronics industry is required. We report a theoretical prediction to identify halogenated silicon films as excellent candidates, which demonstrate high stability, flexibility, and tunable spin-orbit coupling (SOC) gaps up to  $\sim 0.5$  eV under minimal strain below 3%. The extraordinary SOC strength is mainly contributed by the  $p$ -orbital of heavy halogen atoms hybridized with the  $p_{x,y}$ -orbitals of Si scaffold, and thus can be easily manipulated by strain (being  $\sim 100$  times more effective than in silicene) or substrate. Not only the instability problem of silicene for real applications is solved, but also it provides a new strategy to drastically enhance SOC of light-element scaffolds by orbital hybridization. The silicon-based QSH insulator is most promising for developing next-generation, low-power consumption nanoelectronics and spintronics at ambient conditions.

Copyright © EPLA, 2016

**Introduction.** – Topological insulators (TI) are an intriguing new class of quantum matter, which exhibit both an insulating bulk property and conductive edge states in one material, due to the protection of time-reversal symmetry in electronic band structures [1–3]. Spin-orbit coupling (SOC) interactions play a nontrivial role in achieving such a peculiar behavior by enabling helical edge states and suppressing electron backscattering [4]. As a result, the quantum spin hall (QSH) effect can be supported in such materials by a pair of spin-momentum-locked edge states upon breaking up inversion symmetry at edges or surfaces [2,3]. In the past few years both two-dimensional (2D) HgTe-based [5,6] and three-dimensional (3D) Bi<sub>2</sub>Se<sub>3</sub> family [7,8] compounds are first predicted by first principles and then verified in experiments to be QSH insulators. However, most of these materials have very low bulk band gaps opened by SOC interactions, therefore the intriguing Dirac-type surface states can only be

observed at low temperatures  $\leq 10$  K [6]. These materials are also composed by heavy elements which are scarce and often toxic. Large-gap 2D films based on group IV, V and III-V elements in honeycomb structures have been proposed recently [9–20]; however, none of the above materials is considered to be compatible with the current silicon electronics industry, a major factor blockading the potential large-scale implementation of QSH insulators into the existing technology.

To be integrated into the existing electronic circuit applications, low-dimensional materials such as 2D thin films are most desirable. 2D materials have drawn great interest since the first isolation of monolayer graphene in 2004 [21]. The silicon analog of graphene, silicene, with a one-atom-thick honeycomb structure, has been both theoretically predicted [22,23] and experimentally synthesized [24–29]. A major advantage of silicene film is that its manipulation is compatible with the existing silicon electronics. Silicene exhibits a Dirac electron structure around the  $K$ -point and a detectable SOC gap [23], which may yield the QSH effect, due to its low-buckling geometry. However, this

<sup>(a)</sup>Present address: Institute of Physics, Chinese Academy of Sciences - P.O. Box 603, Beijing 100190, China; e-mail: smeng@iphy.ac.cn

Table 1: Structural and electronic properties of the Si-X (X = H, F, Cl, Br, I) film and low-buckled silicene (LB Si).  $a_0$  is the equilibrium lattice constant of the unit cell.  $d_{\text{Si-Si}}$ ,  $d_{\text{Si-X}}$ ,  $\Delta_{\text{Si-Si}}$  denote the Si-Si bond length, Si-X bond length, and the buckling distance in the Si framework, respectively. The cohesive energy  $E_c$  is defined as  $E_c = E_{\text{total}} - E_{\text{silicene}} - E_{\text{X}_2}$ , where  $E_{\text{total}}$ ,  $E_{\text{silicene}}$ ,  $E_{\text{X}_2}$  are the total energy per unit cell of the Si-X film, the free-standing silicene, and the gaseous  $\text{X}_2$  molecule, respectively.  $a_c$  is the critical lattice constant when  $\Delta E_{s-p}$  reaches the zero.  $\varepsilon$  is the corresponding strain defined as  $\varepsilon = (a_c - a_0)/a_0$ .  $a_c$  and  $\varepsilon$  numbers in the parenthesis are the corresponding values with SOC considered.

	I	Br	Cl	F	H	LB Si
$a_0$ (Å)	4.06	3.97	3.94	3.96	3.89	3.86
$d_{\text{Si-Si}}$ (Å)	2.44	2.40	2.39	2.39	2.36	2.28
$d_{\text{Si-X}}$ (Å)	2.48	2.25	2.08	1.63	1.50	–
$\Delta_{\text{Si-Si}}$	0.684	0.710	0.725	0.700	0.719	0.450
Gap (eV)	0.557	1.20	1.28	0.690	2.33	0
$E_c$ (eV/cell)	-2.15	-3.29	-4.08	-8.10	-1.15	0
$a_c$ (Å)	4.25 (4.16)	4.42	4.47	4.49	4.69	–
Strain $\varepsilon$ (%)	+4.7 (+2.5)	+11.3	+13.5	+13.4	+20.6	–

SOC gap of 1.55 meV is too small to support QSH behavior at ambient conditions [23]. Therefore, it is of vital importance to discover silicon-based QSH insulators, with a gap large enough to support room temperature quantum operations.

Here we report a new series of silicon-based films with potential to support ambient QSH effects. These films, comprising monolayer silicene with  $\pi$ -orbitals fully saturated by a halogen or hydrogen termination on both sides of the nanosheet, are energetically stable and mechanically flexible. The biaxial ultimate stress of these Si-X (X = H, F, Cl, Br and I) hybrid films reaches 1.4 GPa and sustains a large tensile strain up to  $\sim 15$ –20%, similar to silicene. A quantum phase transition in electronic structure from trivial insulator to topological insulator is observed when the tensile strain increases to a critical value. When SOC interactions are included, the degenerated  $p_{x,y}$  states at the  $\Gamma$ -point in the Brillouin zone split up and a gap ranging from 0.03 to 0.5 eV is opened. In particular, we found that a Si-I film can potentially support the ambient QSH effect under minimal strains  $\geq 2.5\%$ , due to large SOC gaps. In addition, this SOC gap can be easily tuned by strain, being  $\sim 100$  times more sensitive than that in bare silicene. Different from halogenated tin or germanium films, whereas the states derived from the backbone group IV element dominate, the SOC gap of Si-I films mainly comes from the hybridized  $p_{x,y}$  states of halogen I, which are responsible for the extraordinary large SOC gap and sensitive tunable quantum electronic structure in hybrid Si films. This provides a new strategy to enhance SOC by functionalizing light-element scaffolds. Moreover, the half-silicene, one-side fully hydrogen-saturated silicene, has been produced on a Ag(111) substrate via molecular beam epitaxial growth [30,31], which suggests that the stable, ordered halogenated silicene can be synthesized.

**Results and discussion.** – Density functional theory (DFT) calculations were carried out with Vienna *ab initio* Simulation Package (VASP) [32]. The projector

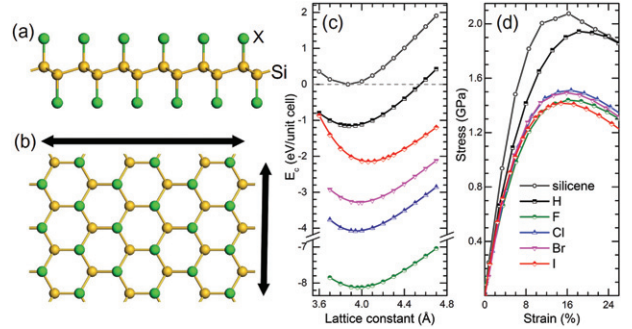


Fig. 1: (Colour online) (a) Side and (b) top views of the optimized halogenated/hydrogenated Si monolayer film. (c) Cohesive energy as a function of the lattice constant for Si-X films. (d) Stress-strain relationship for Si-X films, X = H, F, Cl, Br, I. Results for free-standing silicene are also shown for comparison.

augmented-wave method and the Perdew-Burke-Ernzerhof functional [33] with a kinetic energy cutoff of 500 eV for plane waves are used. Critical electronic structures are further confirmed by the HSE06 hybrid functional [34,35]. A vacuum layer of  $> 14$  Å and  $15 \times 15$   $k$ -points sampling in the in-plane Brillouin zone is employed. All atoms are allowed to relax until the force on each atom is less than 0.01 eV/Å.

Figure 1 shows the atomic structure of halogenated/hydrogenated silicene. A set of X atoms are covalently bonded to the  $p_z$ -orbital of Si atoms above and below the silicene sheet alternately, forming a graphane-like geometry. The optimized lattice constant for Si-X films is  $a_0 = 3.89, 3.96, 3.94, 3.97,$  and  $4.06$  Å for H-, F-, Cl-, Br-, I- terminated films, respectively (see fig. 1 and table 1), all larger than that of free silicene (3.86 Å). Similar to monolayer silicene, the Si-X hybrid sheet also presents a low-buckling geometry, with slightly larger Si-Si interlayer distance of  $\sim 0.7$  Å, 0.2–0.3 Å larger than that in silicene [22]. This distance is however closer to the corresponding values in bulk Si (0.78 Å), implying a  $sp^3$ -like

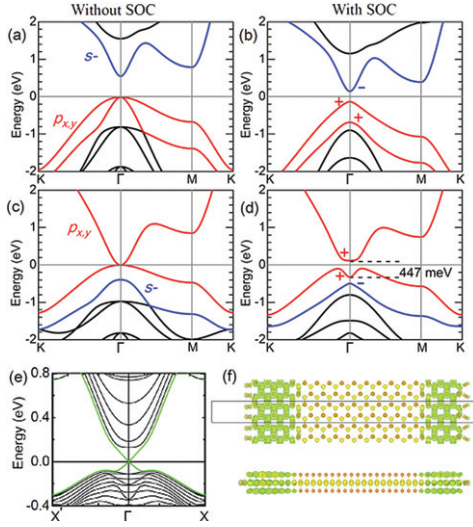


Fig. 2: (Colour online) Band structure for the Si-I film at lattice constant  $a = 4.06 \text{ \AA}$  (a), (b) and  $a = 4.4 \text{ \AA}$  (c), (d). (a) and (c) are calculated without spin-orbit coupling (SOC); while (b) and (d) are calculated with SOC turned on. A direct SOC gap of 447 meV and an indirect bulk gap of 213 meV is observed in (d). The “+” and “-” symbols denote the parity of bands at the  $\Gamma$ -point for Si-I films. (e) The band structure showing topological metallic states (green line) for the saturated Si-I nanoribbon at  $a = 4.4 \text{ \AA}$ , and (f) the corresponding electron density distribution. The black box depicts the supercell used. Both top and side views are shown.

hybridization in Si-X films. These results are similar to those of previous reports [36,37]. Interestingly, we note that the buckling in Si-I is the smallest among all Si-X films, which is attributed to the large strain produced by Si-I bonds. Consequently, the Si-Si bond length increases gradually from 2.28  $\text{\AA}$  in bare silicene to 2.44  $\text{\AA}$  in Si-I films, suggesting the weakening in the in-plane  $\sigma$  bond of the silicene honeycomb lattice.

The cohesive energy of Si-X films is large, being 1.15, 8.10, 4.08, 3.29, 2.15 eV per unit cell for  $X = \text{H}, \text{F}, \dots, \text{I}$  respectively, relative to free-standing silicene and gaseous  $X_2$  molecules. Instead of forming  $\pi$  and  $\pi^*$  bands in silicene, the Si  $p_z$ -orbitals in Si-X films are saturated by X, resulting in a strong covalent Si-X bond with strength of 2.84, 5.23, 3.58, 2.93, and 2.23 eV, for  $X = \text{H}, \text{F}, \dots, \text{I}$ , respectively, comparable to the corresponding X-X bond strength. Desorbing  $X_2$  molecules is energetically unfavored and blocked by a large kinetic barrier. These films are still energetically stable even with a large strain about 15%. A detailed analysis of stress-strain relationship shows that the ultimate biaxial stress is larger than 1.4 GPa and the films can sustain a tensile strain of up to 15–20% for all cases (fig. 1(d)). For comparison, bare silicene, which has been successfully grown on a variety of substrates in MBE experiments [24–29], has an ultimate stress of 2.1 GPa at strain  $\varepsilon = 16\%$ . Moreover, because all of the active  $\pi$  and  $\pi^*$  Si bands have been saturated by the  $p_z$ -orbital of terminal X atoms, these Si-X films

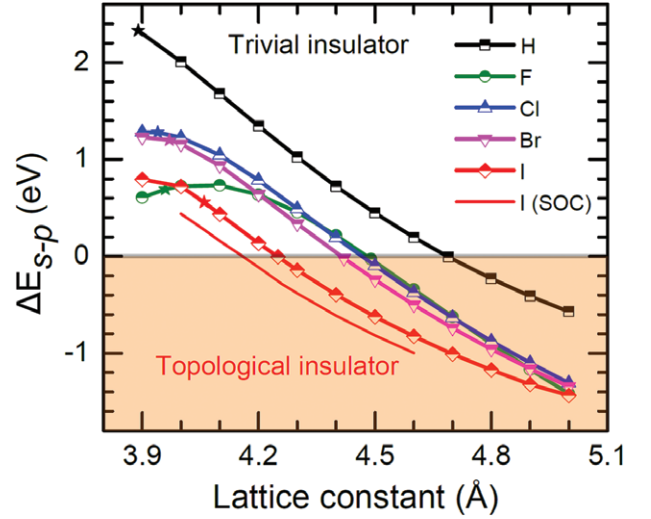


Fig. 3: (Colour online) Energy gap between  $s^-$  and (upper)  $p_{x,y}$ -orbital at the  $\Gamma$ -point,  $\Delta E_{s-p}$ , as a function of the lattice constant for Si-X films. Stars denote the equilibrium lattice constant of the respective film. The thin line is with SOC considered.

are chemically inert and only interacting weakly with the substrate.

Representative electronic band structures of the Si-X film are shown in fig. 2(a), (b), taking Si-I film as an example. Since the Si  $p_z$ -orbital is covalently saturated by the presence of X atoms, the graphane-like geometry would eliminate the  $\pi$  and  $\pi^*$  bands. Thereby, the Dirac cone in the band structure at the  $K$ -point in the Brillouin zone disappears. Instead, a large gap  $> 4 \text{ eV}$  evolves at the  $K$ -point. Consequently, all Si-X films become a semiconductor with a direct band gap at the  $\Gamma$ -point. The band analysis indicates that the conduction band minimum (CBM) is originated from antibonding  $s^-$ -orbitals of Si atoms [9]; while the valence band maximum (VBM) contains two doubly degenerated states resulted from the hybridization of  $p_{x,y} = p_x \pm ip_y$  orbitals of Si and the  $p_{x,y}$  orbitals of I (see fig. S1 in [38]). The energy gap between these two types of orbitals,  $s^-$  and  $p_{x,y}$ , defined as  $\Delta E_{s-p}$  hereafter, accounts for the overall bulk band gap of the Si-X film.

Interestingly, the energy separation between  $s^-$  and  $p_{x,y}$  states  $\Delta E_{s-p}$  is very sensitive to the strain applied. With increasing tensile strain, the  $\Delta E_{s-p}$  becomes smaller and reaches zero at a critical strain value, as displayed in fig. 3. Under even greater strain, the  $s^-$ -orbital becomes lower in energy than the degenerate  $p_{x,y}$  states and now becomes occupied. As a result, electrons in one of the degenerate  $p_{x,y}$  states have to be removed and the state is emptied to maintain charge neutrality. This leads to the fact that the Fermi level, separating occupied and unoccupied bands, is now located exactly at the band crossing of the two  $p_{x,y}$  degenerate states. Therefore, the biaxial strain applied to the Si-X film would introduce an electronic transition from a gapped semiconductor to a zero-gap semi-metal. From

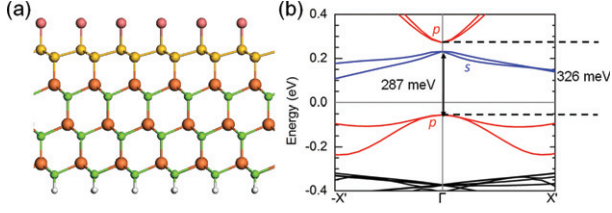


Fig. 4: (Colour online) (a) The Si-I film supported on Cd-terminated CdSe substrate. For effective binding on the substrate, the bottom I layer is removed and the bottom Se layer is saturated by H. (b) Band structure around the  $\Gamma$ -point with SOC included.

DFT calculations, this transition takes place at a critical lattice constant of  $a_c = 4.25, 4.42, 4.47, 4.49,$  and  $4.69 \text{ \AA}$  for  $X = \text{I, Br, Cl, F, and H}$ , respectively (without SOC included).

When SOC interactions are turned on, the degenerate  $p_{x,y}$  states split into two separate bands at the  $\Gamma$ -point and open up a SOC band gap (fig. 2(b), (d)). In this case, we define the energy separation  $\Delta E_{s-p}$  as the energy level difference between the  $s^-$ -orbital and the upper  $p_{x,y}$  band split by SOC. When  $\Delta E_{s-p}$  reaches a negative value, the band inversion occurs and the Si-X film becomes a topological insulator. The typical band structure of Si-I film at the lattice constant of  $4.4 \text{ \AA}$  is shown in fig. 2(d). Under the strain, the  $s^-$ -orbital becomes occupied with a negative  $\Delta E_{s-p}$ . The splitting between two  $p_{x,y}$  orbitals yields a large global SOC gap of  $213 \text{ meV}$ . The electronic structures are qualitatively reproduced by the HSE06 hybrid functional (fig. S2 in [38]). We note that the strained Si-I films are topological insulators which can be directly characterized by the nontrivial  $Z_2$  number (table S1 in [38]). The topological property is also confirmed by the presence of a pair of Dirac-type helical edge states for Si-I nanoribbons, as a result of the band symmetry with respect to spin and momentum degrees of freedom (fig. 2(e), (f)). Because of the protection of time-reversal symmetry, the breakup of inversion symmetry at the film edges results in metallic edge states with locked spin and momentum orientation within the energy gap opened by SOC [2,3]. Since a different spin component is locked with different momentum orientation, these materials suppress electron backscattering in conductive edge states, supporting the quantum spin Hall effect, and are thus called QSH insulators [6].

We found that the critical strain where the transition from a trivial semiconductor to a 2D topological QSH insulator occurs is different for different Si-X films. In particular, a Si-I film can reach the QSH effect with the smallest strain at a lattice constant of  $4.16 \text{ \AA}$  ( $4.37 \text{ \AA}$  by HSE06 functional) when the SOC is turned on. Compared to its equilibrium lattice constant  $a_0 = 4.06 \text{ \AA}$ , this strain is minimal, amounting to  $2.46\%$ . Under tensile strain, band inversion occurs between  $s^-$  and  $p_{x,y}$  states simply because the  $\sigma$ -like bonds between Si  $3s$ -orbitals are much weakened

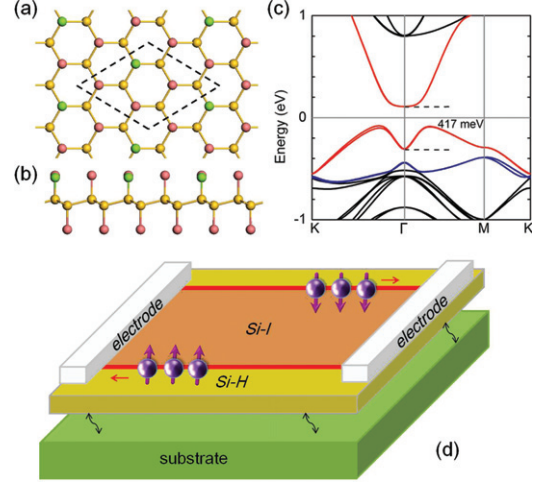


Fig. 5: (Colour online) (a) Top and (b) side views of the Si-I film with  $12.5\%$  Br impurities at a lattice constant of  $4.4 \text{ \AA}$ . Yellow, orange and green spheres denote Si, I and Br, respectively. Dashed lines denote the supercell used. (c) Corresponding band structure plot with SOC included. The direct gap of  $417 \text{ meV}$  is opened by SOC, and the bulk indirect gap is  $189 \text{ meV}$ . (d) Schematic setup for QSH measurement on patterned Si-I/Si-H films anchored on the substrate through bonding at impurity sites (double-head arrows). Vertical arrows show the spin orientation of electrons in the edge states and horizontal arrows show their transport directions.

with the tensile strain, leading to a sharp decrease in the orbital energy of  $s^-$  antibonding states, while  $p_{x,y}$  bonding states are up-shifted in energy instead (fig. S3 in [38]).

This small strain can be easily achieved via epitaxial film growth on substrates such as CdSe, mechanical stretch, or nanoindentation as demonstrated for graphene in the experiment [39]. As an example, we explicitly demonstrate in fig. 4 that Si-I films grown on a Cd-terminated CdSe(111) substrate fulfill this requirement. Even the film with only its upper surface terminated by I is acceptable for this purpose. This setup exerts a large strain onto a Si-I film since the experimental lattice constant of CdSe(111) is  $4.37 \text{ \AA}$ . Through band structure calculations we found that the topological property is well preserved in the epitaxial Si-I film, exhibiting a SOC splitting of  $326 \text{ meV}$  between  $p_{x,y}$  states and a direct gap of  $287 \text{ meV}$  at the  $\Gamma$ -point. In addition, considering multiple complications in the MBE fabrication process, we also address potential effects in the presence of impurities. We found that even with a high density of Br impurities ( $12.5\%$ ), the band structure and the large SOC gap of the Si-I film is unchanged in the presence of defects (fig. 5). The SOC energy splitting and indirect bulk gap is  $417 \text{ meV}$  and  $189 \text{ meV}$ , respectively, for the Si-I film with  $12.5\%$  Br impurity, only slightly reduced from the corresponding values for a perfect Si-I film ( $447 \text{ meV}$  and  $213 \text{ meV}$ ). The tolerance of the topological band structures to defects and impurities implies that the fully saturated Si-I film can be anchored onto substrates through binding

at defect sites, exerting strains without deteriorating its topological properties, so that a QSH measurement can be carried out in a hypothetical setup schematically shown in fig. 5(d). Moreover, the metallic edge states are immune to the presence of non-magnetic impurities because of the protection of time-reversal symmetry.

Strikingly, the band gap induced by SOC in the Si-X films is extraordinarily larger than that expected for Si-based materials [23]. The energy level splitting induced by SOC reaches 0.52 eV for Si-I at a lattice constant of 4.16 Å. Such a SOC gap is 2 orders of magnitude larger than that in pristine low-buckled silicene films (1.55 meV) [23]. It even exceeds the SOC gaps in 3D Bi<sub>2</sub>Se<sub>3</sub> (0.3 eV) [7,8] and the newly proposed honeycomb Sn-X films (0.3 eV) [9,10], making it ideal for realizing the room temperature QSH effect. It is also significantly larger than the intrinsic SOC strength of atomic Si (34 meV) [23]. This is in radical contrast to the Sn-X/Ge-X cases where atomic SOC of backbone Sn/Ge is larger than or comparable to the SOC gap of the film. The SOC gap at the  $\Gamma$ -point is only slightly changed (from 447 to 427 meV) when the Hubbard onsite energy  $U = 2$  eV is turned on (fig. S4 in [38]). Most importantly, such a material is fully compatible with the current electronics industry based on silicon technology.

We note that besides the most promising Si-I film, other types of Si-X material are also meritorious. For instance, the SOC energy gap is 142, 43, and 29 meV for Si-Br, Si-Cl, Si-F at lattice constant  $a = 4.5$  Å, and 24 meV for Si-H at lattice constant  $a = 4.7$  Å, all are intrinsic QSH insulators. All these gap values are larger than or comparable to the characteristic thermal activation energy of 25.8 meV at 300 K. However, a relatively large strain has to be applied to the equilibrium structure to achieve the quantum transition from a trivial semiconductor to a QSH insulator. Molecular-dynamics (MD) simulations explicitly show that strained Si-X films are thermodynamically stable without decomposition or noticeable deviation in its honeycomb lattice at 300 K. No obvious negative frequencies were detected from phonon dispersion calculations, except that the small imaginary frequency in the transverse acoustical phonon branch around the  $\Gamma$ -point, which is less than  $8 \text{ cm}^{-1}$ , comes from numerical inaccuracy (fig. S5 in [38]).

It is commonly believed that materials composed by light elements such as carbon and silicon have very small SOC strength, rendering them unsuitable to support the QSH effect at ambient temperature. To achieve a large-gap QSH insulator, 2D and 3D materials made of heavy elements such as Hg and Bi are sought out to ensure strong SOC [2–8]. Following this line of thinking, an artificial honeycomb lattice based on heavy-element tin was proposed as a new platform to achieve ambient QSH behaviors and spintronic devices [9,10]. However, the present work implies that it is plausible to use light elements to form a large-gap QSH insulator via orbital hybridization. Enlightened by this new insight, honeycomb lattices made of heavy elements are not necessary. This fact will bring

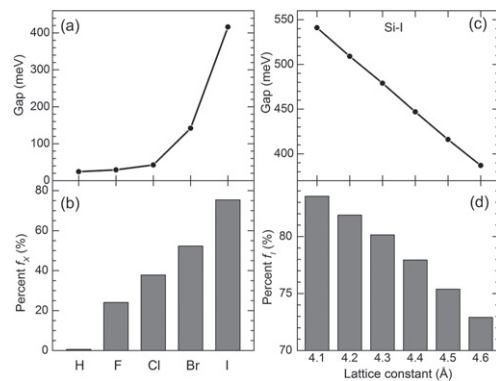


Fig. 6: (a) The energy gap opened by spin-orbit coupling and (b) the percentage of the orbital contribution in the  $p_{x,y}$  bands from X atoms,  $f_x$ , in the Si-X films at a lattice constant of 4.5 Å (4.7 Å for Si-H). (c) The energy gap in the  $p_{x,y}$  bands split by spin-orbit coupling and (d) the percentage of the orbital contribution from I atoms as a function of the lattice constant in the Si-I film.

out new strategies and opens new possibilities for designing functionalized quantum materials.

In contrast to the common belief that strong SOC comes from the 2D scaffold material that forms the honeycomb lattice [9,10], we found that the large SOC band gap can be achieved by orbital hybridization between the honeycomb lattice of light elements (such as Si) and a layer of terminating heavy elements (such as I). The analysis of the orbital contribution to the  $p_{x,y}$  bands shows that the major contribution up to 70–85% comes from the  $p_{x,y}$ -orbitals of I in a Si-I film, while for a Si-H film the H orbital contributes only negligibly, by less than 10% (see fig. 6(a)). For F-, Cl-, and Br-terminated silicene, orbital contribution from halogen  $p$ -orbitals ranges from 20% to 50%. Due to the dominant presence of I states in hybrid  $p_{x,y}$  states, the SOC strength in the Si-I film is much enhanced than that for pristine silicene films. We note that the intrinsic SOC strength for the Si element is 34 meV [23] and for I it is  $\sim 0.7$  eV. At the lattice constant  $a = 4.3$  Å (corresponding to a tensile strain  $\varepsilon = 5.9\%$ ), Si-I is a true QSH insulator with the SOC energy splitting between the two  $p_{x,y}$  states being 0.48 eV and a usable bulk gap between the unoccupied  $p_{x,y}$  band and the occupied  $s^-$  band of  $\sim 0.2$  eV, favoring the ambient temperature QSH effect.

Interestingly, we found that the SOC band gap can be easily tuned by the applied strain. Among the cases studied, the SOC energy splitting is largest, 552 meV for the Si-I film at the equilibrium lattice constant  $a = 4.06$  Å, while it reduces to 387 meV at the lattice constant  $a = 4.6$  Å. There is an approximate linear relationship between the SOC splitting and the lattice constant (and thus the strain) of Si-I film. This linear dependence is attributed to the level of hybridization between Si and I  $p_{x,y}$ -orbitals, which also increases linearly with shrinking lattice constant (fig. 6(b)). This fact implies that strain engineering is not only an effective way to introduce

topological phase transitions, but also could well tune the SOC strength. We further note that this strategy is not limited to Si-X films. Pristine monolayer silicene and Sn-X films can also develop a larger SOC gap under compressive strain. However, the sensitivity of the SOC gap responding to strain is unparallel in the present case, rendering a change of 14.5 meV in the SOC gap with 1% strain change, compared to 0.25 meV per 1% strain in silicene [23] and 3.6 meV per 1% strain in the Sn-F film [9].

Now we discuss potential fabrication routes for the proposed halogenated silicene films. Several previous works have already reported the study on the stability and synthesis of hydrogenated silicene [30,31,40]. Single-layer silicene films can be grown by evaporating silicon atoms from a silicon wafer onto a preheated metal substrate such as Ag(111) [24,25]. Adsorption of foreign atoms onto silicene can be performed by exposing the sample at room temperature to a high-purity hydrogen or halogen gas. Previous results clearly show that hydrogen atoms are strongly adsorbed onto silicene surface forming a highly ordered pattern and remain stable [30,31]. We expect that full coverage of H and halogen atoms on both sides of silicene is possible under optimal growth conditions and/or on proper substrates. Indeed scattered small patches of fully hydrogenated Si films were observed, whose strict confirmation is subject to future experiment [30,31].

**Conclusions.** – In summary, we identify a new class of silicon-based QSH insulators, which have very large SOC gaps up to 0.4–0.5 eV under minimal strain larger than 2.5%. Different from conventional TI materials, the large SOC does not come from the Si honeycomb scaffold but it is mainly contributed by the saturating halogen elements, making it  $\sim 100$  times more sensitive to the applied strain than bare silicene. These films, while compatible with the existing Si industry, are thermodynamically stable and flexible, and can sustain large strains with easily tunable phase transitions and quantum properties, making them very promising for the next-generation nanoelectronics and electromechanical applications, exemplified by the room temperature QSH effect.

\*\*\*

This work was supported by “973” Project of China (2015CB921001 and 2012CB921403), NSFC (grants 11304176 and 11222431), and CAS (grant XDB070301).

## REFERENCES

- [1] HALDANE F. D. M., *Phys. Rev. Lett.*, **61** (1988) 2015.
- [2] HASAN M. Z. and KANE C. L., *Phys.*, **82** (2010) 3045.
- [3] QI X.-L. and ZHANG S.-C., *Rev. Mod. Phys.*, **83** (2011) 1057.
- [4] KANE C. L. and MELE E. J., *Phys. Rev. Lett.*, **95** (2005) 226801.
- [5] BERNEVIG B. A. *et al.*, *Science*, **314** (2006) 1757.
- [6] KOENIG M. *et al.*, *Science*, **318** (2007) 766.
- [7] ZHANG H. *et al.*, *Nat. Phys.*, **5** (2009) 438.
- [8] XIA Y. *et al.*, *Nat. Phys.*, **5** (2009) 398.
- [9] XU Y. *et al.*, *Phys. Rev. Lett.*, **111** (2013) 136804.
- [10] MA Y. *et al.*, *J. Phys. Chem. C*, **116** (2012) 12977.
- [11] MA Y. *et al.*, *J. Mater. Chem.*, **22** (2012) 12587.
- [12] SI C. *et al.*, *Phys. Rev. B*, **89** (2014) 115429.
- [13] SONG Z. *et al.*, *NPG Asia Mater.*, **6** (2014) e147.
- [14] HUANG Z. *et al.*, *New J. Phys.*, **16** (2014) 105018.
- [15] CHOU B.-H. *et al.*, *New J. Phys.*, **16** (2014) 115008.
- [16] LIU C.-C. *et al.*, *Phys. Rev. B*, **90** (2014) 085431.
- [17] HUANG Z.-Q. *et al.*, *Phys. Rev. B*, **88** (2013) 165301.
- [18] CHUANG F.-C. *et al.*, *Appl. Phys. Lett.*, **102** (2013) 022424.
- [19] CRISOSTOMO C. P. *et al.*, *Nano. Lett.*, **15** (2015) 6568.
- [20] JIN K.-H. and JHI S.-H., *Sci. Rep.*, **5** (2015) 8426.
- [21] NOVOSELOV K. S. *et al.*, *Science*, **306** (2004) 666.
- [22] CAHANGIROV S. *et al.*, *Phys. Rev. Lett.*, **102** (2009) 236804.
- [23] LIU C.-C. *et al.*, *Phys. Rev. Lett.*, **107** (2011) 076802.
- [24] CHEN L. *et al.*, *Phys. Rev. Lett.*, **109** (2012) 56804.
- [25] FENG B. J. *et al.*, *Nano Lett.*, **12** (2012) 3507.
- [26] VOGT P. *et al.*, *Phys. Rev. Lett.*, **108** (2012) 155501.
- [27] FLEURENCE A. *et al.*, *Phys. Rev. Lett.*, **108** (2012) 245501.
- [28] MENG L. *et al.*, *Nano Lett.*, **13** (2013) 685.
- [29] CHEN L. *et al.*, *Phys. Rev. Lett.*, **110** (2013) 85504.
- [30] QIU J. *et al.*, *ACS Nano*, **9** (2015) 11192.
- [31] QIU J. *et al.*, *Phys. Rev. Lett.*, **114** (2015) 126101.
- [32] KRESSE G. and FURTHMULLER J., *Phys. Rev. B*, **54** (1996) 11169.
- [33] PERDEW J. P. *et al.*, *Phys. Rev. Lett.*, **77** (1996) 3865.
- [34] HEYD J. *et al.*, *J. Chem. Phys.*, **118** (2003) 8207.
- [35] HEYD J. *et al.*, *J. Chem. Phys.*, **124** (2006) 219906.
- [36] GAO N. *et al.*, *Phys. Chem. Chem. Phys.*, **14** (2012) 257.
- [37] WANG Y. and DING Y., *Solid State Commun.*, **155** (2013) 6.
- [38] The supporting information is available free of charge via the Internet at [http://everest.iphy.ac.cn/papers/Si-X\\_supplementalMaterial.pdf](http://everest.iphy.ac.cn/papers/Si-X_supplementalMaterial.pdf).
- [39] LEE C. *et al.*, *Science*, **321** (2008) 385.
- [40] WU W. C. *et al.*, *J. Mater. Chem. C*, **3** (2015) 2593.